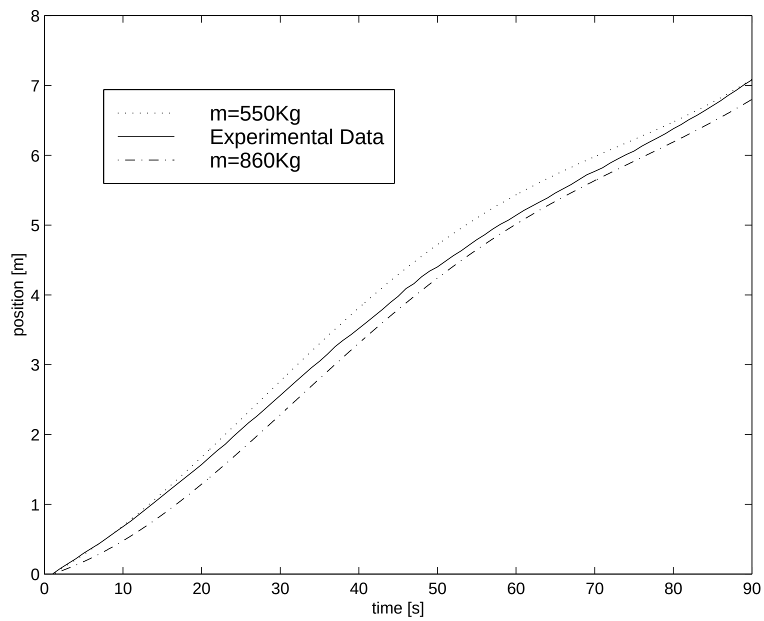

4.32.Experimnetal and simulated data relative to the input force of experiment SUI1. Simulated data refers to the m displayed and $k_u = 38Ns/m$, $k_{u|u|} = 333Ns^2/m^2$.

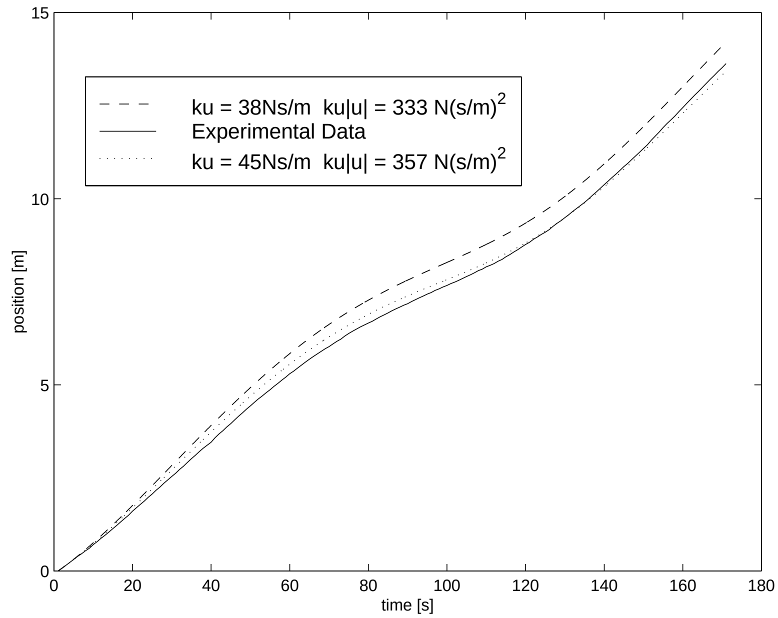

4.33.Experimnetal and simulated data relative to the input force of experiment SUI2. Simulated data refers to $m = 705Kg$ and to the displayed drag coefficients.

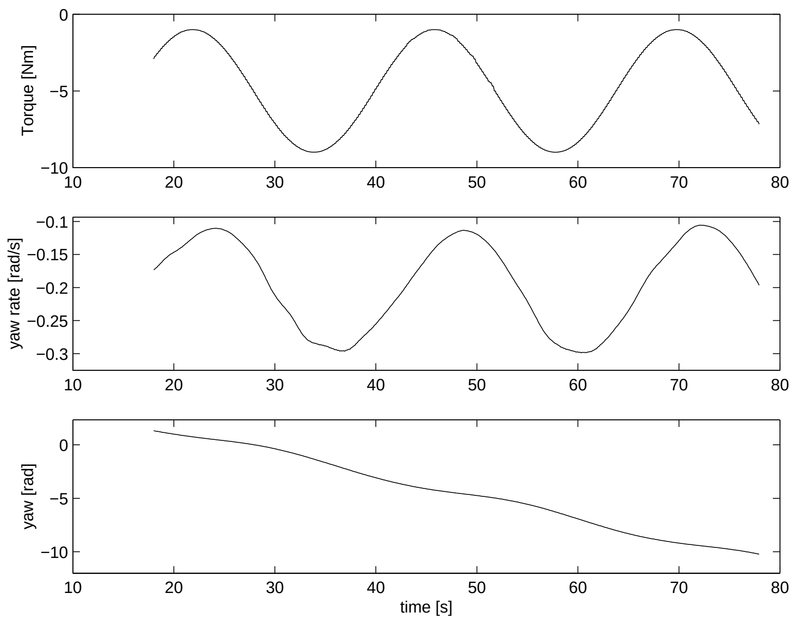

4.34.Yaw inertia parameter identification experimentYAI1.

being I_z ROMEOs z-axis moment of inertia, f the applied torque as given by equation (4.40) and k_r the full efficiency yaw drag coefficient $k_r = 35Nms/rad$. The time constant $\tau = I_z/k_r$ of equation (4.46) can be a priori estimated replacing for I_z the moment of inertia, along the its height, of a parallelepiped having a uniformly distributed $450Kg$ mass, width $1.3m$, length $0.8m$, i.e. $I_z = \frac{1}{12}450(0.8^2 + 1.3^2) \simeq 87.38Kgm^2$. The corresponding input frequency, according to equation (4.39), is

$$\omega_{opt} = \frac{k_r}{\sqrt{3}I_z} \simeq 0.23Hz \tag{4.47}$$

Two different experiments, labeled YAI1 (YAw Inertia) and YAI2, will be considered. During the YAI1 experiment the input torque was provided by the only rear left and front right thrusters (figure (4.3)), so that unit efficiency is assumed to hold for negative velocity and torques. In accordance with equation (4.47), the input torque frequency during the YAI1 experiment has been chosen to be $\omega = 0.26Hz$ and the applied torque f in Nm was

$$f = -5 + 4\sin(0.26t)$$

in order to avoid propeller inversions. The position was measured with a $10Hz$ sampling rate compass and the velocity has been computed with an off line 4^{th} order Savitzky-Golay filter having a symmetric window of full length 41 points. The input torque,

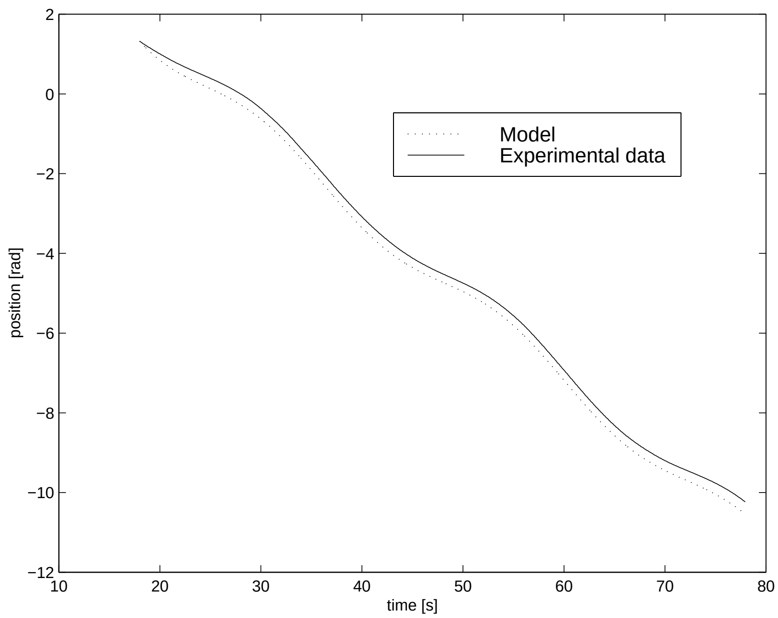

4.35.Experiment YAI1 measured position and expected model position with $k_r = 35Nms/rad$, $I_z = 93Kgm^2$.

the filtered yaw rate and the yaw measurement of the YAI1 experiment are reported in figure (4.34). Implementing the estimation algorithm described in section (4.2.8) yields

$$\text{YAI1 experiment: } I_z = (93.0 \pm 0.6)Kgm^2$$

being the estimation error computed with the usual technique based on equations (4.12) and (4.6) probably underestimated for the reasons outlined in the previous two sections. Nevertheless the identified model performance is acceptable, as shown in figure (4.35) where the experimental position data of experiment YAI1 are compared with the model predicted position. The YAI2 experiment refers to an input torque signal of frequency $\omega = 0.39Hz$ provided by the front left and rear right thrusters. Torque unit efficiency is assumed for positive torques and velocities, so the input torque signal was

$$f = 5 + 4\sin(0.39t)$$

The angular (yaw) position was measured with a $10Hz$ sampling rate compass and, as for the YAI1 experiment, yaw rate has been computed with an off line 4^{th} order Savitzky-Golay filter having a symmetric window of full length 41 points. Applied torque, computed velocity and measured position of experiment YAI2 are reported in figure (4.36). The resulting estimated value of the inertia I_z according to the experiment

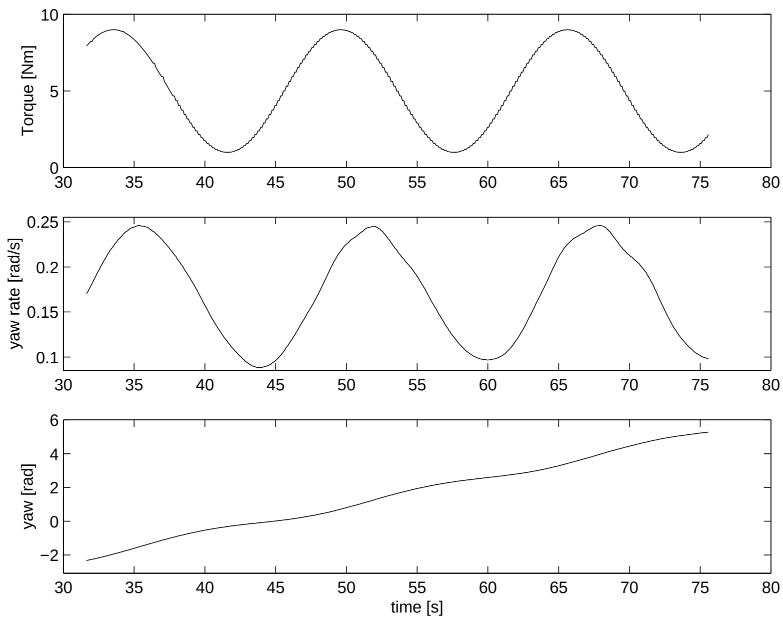

4.36.Yaw inertia parameter identification experimentYAI2.

YAI2 is

$$\text{YAI2 experiment: } I_z = (100.0 \pm 0.7)Kgm^2$$

4.3 Summary

Within this chapter an identification procedure for the drag and inertia parameters of an open frame ROV and the results of its implementation on a real system have been presented. The identification procedure is based on on-board sensor data rather then towing tank experiments. Although in principle towing tank methods allow a better estimation accuracy (in particular of the inertia coefficients), they are usually performed on a scaled model of the vehicle rather then on the real system [73] with all the related drawbacks. Moreover such towing tank methods are much more expensive, complex and time consuming. A simple set of inputs and the relative model fitting technique have been defined for the on board sensor based estimation of drag and inertia coefficients of a decoupled ROV model: the major advantage of the proposed approach consists in the possibility of estimating the propeller-hull and propeller-propeller efficiency parameters that would be otherwise unobservable. Moreover thanks to their simple nature the tests may be repeated when the vehicle changes configuration in or-

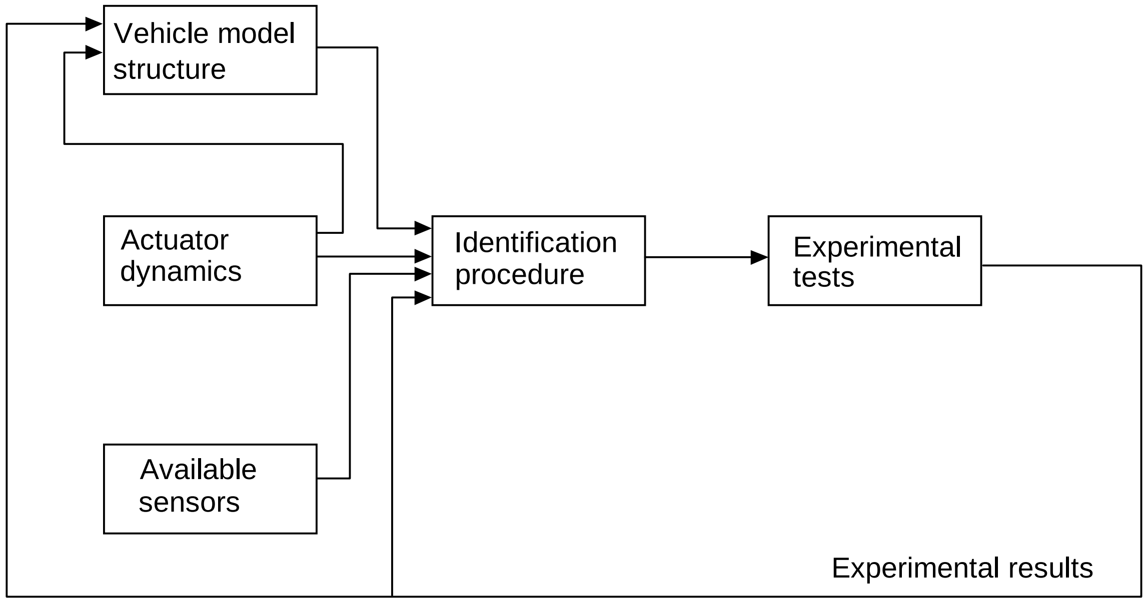

4.37.Rationale of the identification procedure design.

der to tune the control and navigation systems when required. It is worthwhile pointing out that the identification procedure has been designed taking into account the vehicle model structure, the type of available sensors and the actuator dynamics. Moreover during the experimental implementation of such procedure on the ROMEO ROV both the system model and the identification procedure itself have been “tuned” on the basis of the experimental results. The logical flow chart of the work described in this chapter is reported in figure (4.37). The developed procedure has been adopted to estimated the drag and inertia coefficients and their variances for the surge, sway, heave and yaw axis of the ROMEO ROV: the data relative to numerous experimental trials has been processed and the results are reported in detail. It has been shown that yaw drag in the typical operating yaw rate range, i.e. $|\dot{\psi}| \leq 10\,\deg/s$, is better modeled by an only linear term rather then both a linear and quadratic one: this is important as it suggests that as far as the yaw axis is concerned linear control techniques may be successfully adopted. At last it has been shown that the propeller-hull and propeller-propeller interactions may have a most important relevance in the dynamics of open frame ROVs and should thus be taken explicitly into account. To this extent an efficiency parameter, closely related to the thruster installation coefficient described by Goheen et al.[66], has been introduced and its value and variance have been estimated in all the cases of interest.

Chapter 5
Motion control and path planning

In this chapter some original results regarding the motion control and path planning of nonholonomic systems with reference to underwater vehicles will be outlined.

5.1 2D motion control of a nonholonomic vehicle

Three major issues of robot motion control are the state stabilization problem, the path generation problem and the path tracking problem. If the system at hand has nonholonomic constraints, as for wheeled vehicles or under-actuated underwater vehicles, these problems are particularly challenging. The literature regarding the stabilization of nonholonomic systems is very large and, as a detailed overview of the topic goes beyond the possibilities of this work, only the results of interest will be here reported. For a wider discussion of the current state of the art in the control of nonholonomic systems refer to [74] [75] [76]. The main difficulty in the stabilization of nonholonomic systems is related to the theorem of Brockett [77]:

Theorem (Brockett, 1983) *Given* $\dot{q} = G(q)u$ *with* $g(q_0)u_0 = 0$ *and* $g(\cdot)$ *continuously differentiable in a neighborhood of* q_0*, then there exists a time invariant continuously differentiable control law which makes* (q_0, u_0) *asymptotically stable if and only if* $\dim(q) = \dim(u)$.

Indeed many systems of practical interest may not be asymptotically stabilized via smooth time invariant feedback due to this result. Among these the unicycle kinematic model:

$$\begin{aligned} \dot{x} &= u \cos \phi \\ \dot{y} &= u \sin \phi \\ \dot{\phi} &= \omega \end{aligned} \tag{5.1}$$

being x, y the Cartesian coordinates with respect to the inertial frame $< 0 >$, u the linear velocity, ϕ the orientation with respect to the x-axis and ω the angular velocity as shown in figure (5.1). To tackle this difficulty most authors have focused their attention either on smooth but time varying state feedback approaches, or on time independent but noncontinuous state feedback approaches. As far as underwater vehicles are concerned examples of such control laws are provided by Egeland et al.[78] and Pettersen et al.[79]. A most interesting way of analyzing the asymptotic stabilization of the unicycle model given by equation (5.1) is related to a remark of the above cited Brockett Theorem given

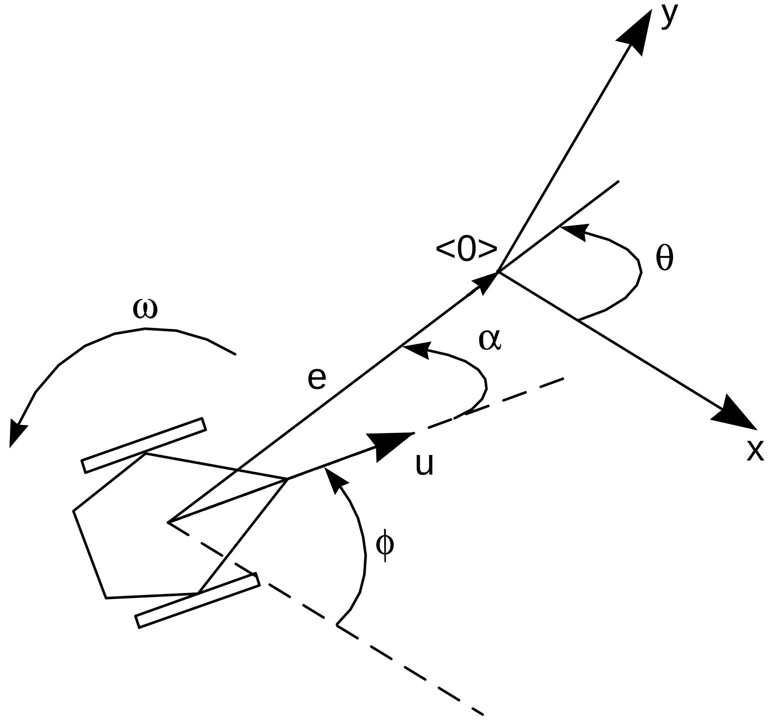

5.1.Unicycle kinematics

by the same Brokcett [77]: *"If we have*

$$\dot{q} = \sum_{i=1}^{m} g_i(q)u_i : q(t) \in \Re^n$$

with the vectors $g_i(q)$ *being linearly independent at* q_0 *then there exists a solution to the stabilization problem if and only if* $m = n$. *In this case we must have as many control parameters as we have dimensions of* q. *Of course the matter is completely different if the set* $\{g_i(q_0)\}$ *drops dimension precisely at* q_0*."* As shown by the works of Casalino et al.[1] and Badreddin et al.[80] , this last observation plays a key role in the solution of the unicycle stabilization problem: if the unicycle kinematics is represented in polar-like coordinates

$$\begin{aligned} e &\triangleq \sqrt{x^2+y^2} \\ \theta &\triangleq ATAN2(-y,-x) \\ \alpha &\triangleq \theta - \phi \end{aligned} \tag{5.2}$$

as shown in figure (5.1) Brocketts Theorem does not hold anymore as the state itself is not defined for $e = 0$. With this choice of the state variables the state equations are

$$\begin{aligned} \dot{e} &= -u\cos\alpha \\ \dot{\alpha} &= -\omega + u\frac{\sin\alpha}{e} \\ \dot{\theta} &= u\frac{\sin\alpha}{e} \end{aligned} \tag{5.3}$$

and a smooth time invariant state feedback law for global asymptotic stability is not prevented by Brocketts result. Examples of such possible control laws are reported in [1] [2] and [80]. Indeed the idea of simply adopting a different state representation in which Brocketts Theorem does not hold to solve the smooth state feedback global stability problem for general models of nonholonomic systems is very appealing and has been dealt by A. Astolfi [81].

5.1.1 A state feedback solution for the unicycle model

Casalino et al.[1] presented the smooth feedback law

$$u = \gamma\, e\cos\alpha : \gamma > 0 \tag{5.4}$$

$$\omega = k\alpha + \gamma\cos\alpha\frac{\sin\alpha}{\alpha}(\alpha + h\theta) : k,h > 0 \tag{5.5}$$

that globally stabilizes the unicycle system given by equation (5.3) in the origin. A major draw back of this result that prevents its straightforward application to the control of the planar motion of real systems as underwater or air vehicles equipped with actuators

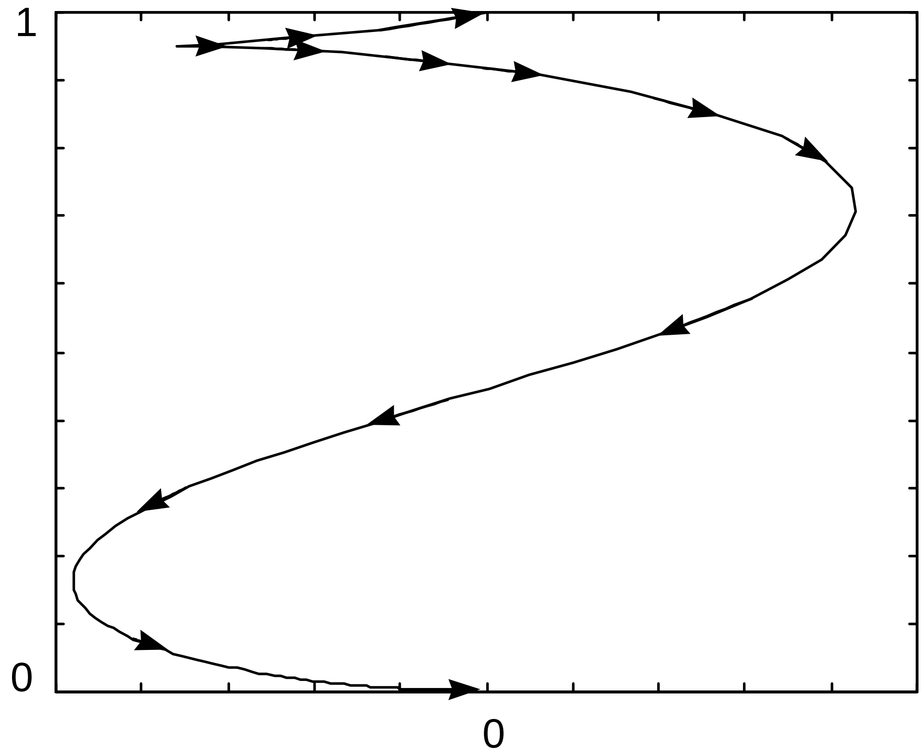

5.2.Initial position $(0, 1)$ with orientation $\phi = \pi/4$.

in only one direction is the unicycle-like nonholonomic constraint according to which angular velocity can be assigned independently. This is equivalent to the obvious statement that a unicycle-like vehicle can turn on itself thus moving on an infinite curvature trajectory, while a wider class of moving systems (like bicycles, cars, torpedoes or airplanes) can only move on bounded curvature paths. To have a qualitative understanding of the behaviour of the above algorithm (equations (5.4) and (5.5)) refer to figures (5.2) and (5.3). Notice that within the unicycle-like approach of Casalino et al.[1] given by equations (5.4) and (5.5) the velocity u can take both positive and negative signs: indeed the resulting path inversion points correspond to null linear velocity u. Moreover the closed loop equation for the position error e is

$$\dot{e} = -\gamma e \cos^2 \alpha$$

showing that e is always decreasing. This is certainly a most interesting aspect of the above outlined algorithm as it guarantees exponential convergence of e. As described in the papers of Caccia et al.[28] [30] and Casalino et al.[82] the control strategy given by equations (5.4) and (5.5) can be successfully adopted for the planar motion control of underwater vehicles that can steer having null surge velocity ($\omega \neq 0, u = 0$), but in

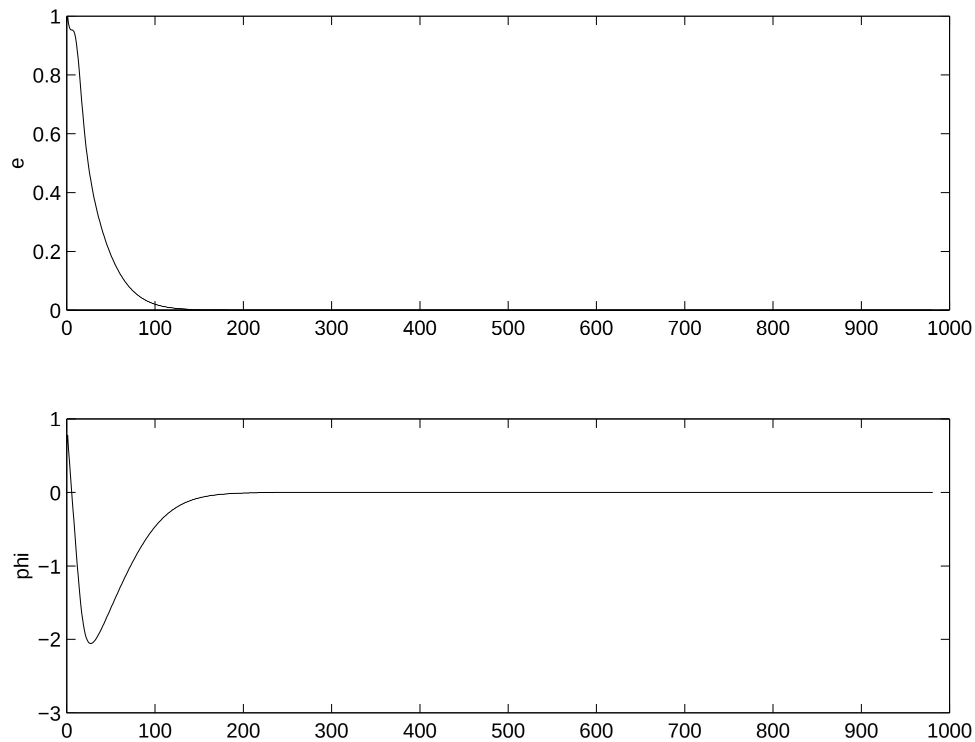

5.3.Errror e and orientation ϕ with respect to time relative to the previous figure.

many underwater vehicle applications the system can (or is preferred to) move in the only forward direction and can not turn with $u = 0$. With these ideas in mind the above outlined approach can be modified to introduce the (bounded) curvature explicitly in the model and to prevent inversions in the sign of the linear velocity u.

5.1.2 A state feedback solution for a more general model

A simple way to introduce the curvature in the unicycle model is to consider the bicycle-like kinematics given, in Cartesian coordinates, by

$$\begin{aligned} \dot{x} &= u \cos \phi \\ \dot{y} &= u \sin \phi \\ \dot{\phi} &= uc \end{aligned} \tag{5.6}$$

being the control signals u and the curvature c. With the polar-like variable choice given in equation (5.2) this model is transformed in the following:

$$\begin{aligned} \dot{e} &= -u \cos \alpha \\ \dot{\alpha} &= -u \left(c - \frac{\sin \alpha}{e} \right) \\ \dot{\theta} &= u \frac{\sin \alpha}{e} \end{aligned} \tag{5.7}$$

Notice that within this model the linear velocity u can not change sign, as when $u = 0$ the state stops moving. Thus in order to converge to the origin of the state space, u can take the null value only in the target state $(0, 0, 0)$. In order to design a globally stable smooth state feedback control law for the system given by equation (5.7) a Lyapunov-like based approach will be followed. The control law synthesis method is inspired by and closely related to the previous works of Casalino et al.[1] and Aicardi et al.[2]. Having noticed that the state equation (5.7) derivative is identically null when $u = 0$ suggests to try the control law

$$u = \gamma e : \gamma > 0 \tag{5.8}$$

The point is now to guarantee, by a suitable choice of c, that within some finite time $\cos \alpha < 0$ (so that e starts decreasing) and asymptotically $(e, \alpha, \theta) \rightarrow (0, 0, 0)$. To calculate c consider the state equation (5.7) given (5.8), i.e.,

$$\begin{aligned} \dot{e} &= -\gamma e \cos \alpha \\ \dot{\alpha} &= -\gamma e \left(c - \frac{\sin \alpha}{e} \right) \\ \dot{\theta} &= \gamma \sin \alpha \end{aligned} \tag{5.9}$$

and the quadratic Lyapunov candidate function

$$V = \frac{1}{2}(\alpha^2 + h\theta^2) : h > 0 \tag{5.10}$$

having time derivative

$$\dot{V} = \alpha\dot{\alpha} + h\theta\dot{\theta} = \gamma(\alpha \sin\alpha + h\theta \sin\alpha - \alpha e c) \tag{5.11}$$

This last equation suggests the choice of c as:

$$c = \frac{\sin\alpha}{e} + h\frac{\theta}{e}\frac{\sin\alpha}{\alpha} + \beta\frac{\alpha}{e} : \beta > 0 \tag{5.12}$$

so that the time derivative of the candidate Lyapunov function V becomes

$$\dot{V} = -\gamma\beta\alpha^2 \leq 0 \tag{5.13}$$

As in the model of Casalino et al. [1] and as will be shown in the sequel, the h parameter in equation (5.10) is needed to guarantee that $\lim_{(e,\alpha)\to(0,0)} c = 0$. Moreover being V positive and radially unbounded equation (5.13) implies that it tends towards a non-negative finite limit, thus

$$\begin{aligned} \lim_{t\to\infty} \alpha &= \bar{\alpha} \\ \lim_{t\to\infty} \theta &= \bar{\theta} \end{aligned}$$

The above and the fact that $\dot{V}$ is uniformly continuous[5] imply by Barbalat's Lemma that $\dot{V}$ tends to zero, so that $\bar{\alpha} = 0$. Substituting equation (5.12) in (5.9) gives:

$$\begin{aligned} \dot{e} &= -\gamma e \cos\alpha \\ \dot{\alpha} &= -\gamma\left(\beta\alpha + h\theta\frac{\sin\alpha}{\alpha}\right) \\ \dot{\theta} &= \gamma \sin\alpha \end{aligned} \tag{5.14}$$

From the facts that $\alpha \to 0$, $\theta \to \bar{\theta}$, and that $\dot{\alpha}$ is uniformly continuous, again by Barbalat's Lemma it follows that the limit

$$\lim_{t\to\infty} \dot{\alpha} = -\gamma h\bar{\theta} = 0$$

and thus the limit value $\bar{\theta}$ of θ must be zero. Moreover notice from the last of equations (5.14) that given the above results also $\dot{\theta}$ tends asymptotically towards zero. The above

[5] $\ddot{V} = -2\gamma\beta\alpha\dot{\alpha}$ is bounded.

results show that

$$\begin{aligned} \alpha &\rightarrow 0\,;\dot{\alpha}\rightarrow 0 \\ \theta &\rightarrow 0\,;\dot{\theta}\rightarrow 0 \end{aligned}$$

so as $t \rightarrow \infty$ there must be some finite value of t, say t^*, starting from which $\cos\alpha < 0$ and thus

$$\dot{e} \rightarrow -\gamma e < 0 \Rightarrow e \rightarrow 0$$

The behaviour of the above developed closed loop control, i.e.,

$$\begin{cases} u = \gamma e : \gamma > 0 \\ c = \dfrac{\sin\alpha}{e} + h\dfrac{\theta}{e}\dfrac{\sin\alpha}{\alpha} + \beta\dfrac{\alpha}{e} : \beta, h > 0 \end{cases} \tag{5.15}$$

depends on the choice of the parameters γ, β, h. In particular while u is obviously limited as long as e and γ are finite, the limit $\lim_{(e,\alpha,\theta)\rightarrow(0,0,0)} c$ must be analyzed: when the state (e, α, θ) approaches the origin $(0, 0, 0)$ the state equations (5.14) can be approximated by the linear system

$$\begin{pmatrix} \dot{\alpha} \\ \dot{\theta} \end{pmatrix} = \begin{bmatrix} -\gamma\beta & -h\gamma \\ \gamma & 0 \end{bmatrix} \begin{pmatrix} \alpha \\ \theta \end{pmatrix} \tag{5.16}$$

$$\dot{e} = -\gamma e \tag{5.17}$$

and

$$c = \frac{\alpha}{e}(1+\beta) + h\frac{\theta}{e}$$

so that in order to reach the target $(0, 0, 0)$ on a straight line (i.e. with null curvature) the real part of the dominant pole of equation (5.16) must be strictly larger then γ. By direct calculation the eigenvalues of the system matrix of equation (5.16) are

$$\lambda_{\pm} = \frac{1}{2}\left(-\gamma\beta \pm \sqrt{\gamma^2\beta^2 - 4h\gamma^2}\right) \tag{5.18}$$

so the requested condition $|\,\mathrm{Re}(\lambda_+)| > \gamma$ is equivalent to

$$h > 1\,;\ 2 < \beta < h + 1$$

Moreover by direct analysis of equation (5.18) it follows that if $h > 1$

$$\Delta \leq 0 \Longleftrightarrow \beta \leq 2\sqrt{h}$$

being $\Delta = \gamma^2\beta^2 - 4h\gamma^2$ so that the system is stable and under damped for $2 < \beta < 2\sqrt{h}$, stable and critically damped for $2 < \beta = 2\sqrt{h}$, stable and over damped for $2\sqrt{h} < \beta < h + 1$. If $h > 1$ and $\beta < 2 \cup \beta > h + 1$ or if $h = 1\ \forall\ \beta$ the curvature diverges as the target state is approached, thus the importance of the h parameter in equation (5.10).

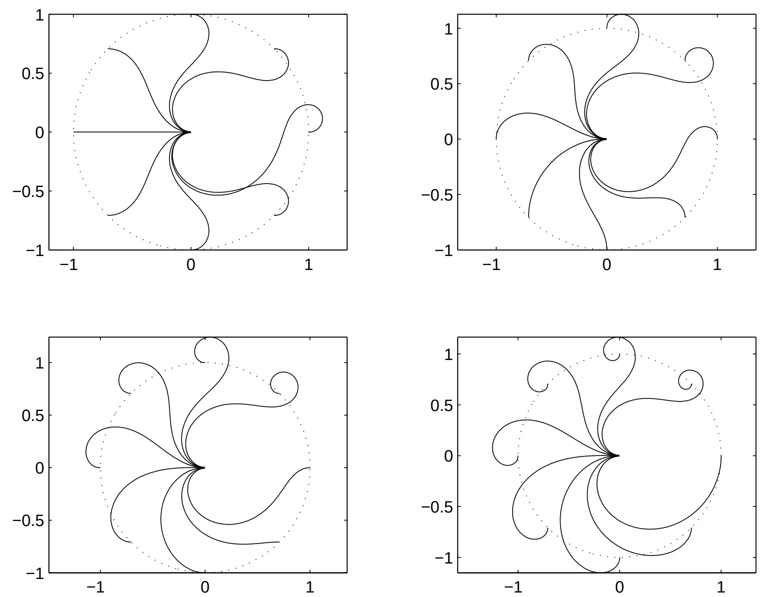

5.4.Paths starting on the unit circle with gains $\gamma = 1,\ h = 2,\ \beta = 2.91$. From left to right and from top to bottom the starting orientation ϕ_0 is: 0, $\pi/2$, π, $3\pi/2$.

A most important property of the proposed algorithm is the boundedness of the control input c. Equation (5.15) shows that $|c| \leq \frac{h\pi+1+\beta|\alpha_{max}|}{e_{min}}$ and that c tends to zero as e grows. The above linear analysis shows that if the gains β and h are suitably chosen c tends to zero also as (e, α, θ) tends to zero. Moreover notice that the linearized system given by equations (5.16) and (5.17) actually holds for small values of α and whatever e and θ are, as the only adopted approximation has been $\sin\alpha \simeq \alpha$ and $\cos\alpha \simeq 1$. As a consequence the only requirement necessary for c to be minor than a prescribed upper bound during the whole state trajectory, is that during the convergence of α in the state space region where $\sin\alpha \simeq \alpha$, the error e is kept larger then some limit value e_{min}. Intuitively this means that if an upper bound $\bar{c}$ is given on c, as in most real systems, the initial error e_0 must be larger then some limit value $e^*(\alpha_0, \theta_0, \bar{c})$ depending on the initial values of α and θ and on $\bar{c}$.

For a qualitative understanding of the resulting paths refer to figures (5.4) and (5.5). In figure (5.4) various paths starting on the unit circle with different orientation are displayed, while figure (5.5) shows the influence of a 2π difference on the initial angular position ϕ_0 on the path. With reference to the above reported stability analysis, all the simulations reported in figures (5.4) and (5.5) are relative to gain values that guarantee a stable and over damped convergence of c to zero, in particular $\gamma = 1$, $h = 2$, $\beta = 2.91$.

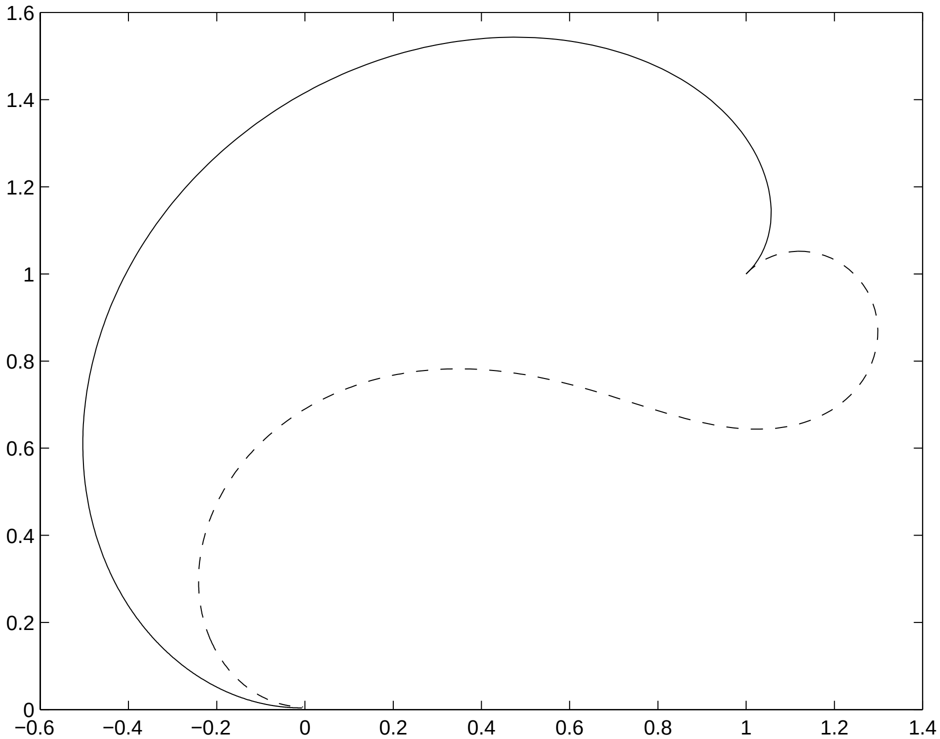

5.5.Paths starting in $(1,1)$ with orientations $\phi_0 = \pi/4$ (dashed line) and $\phi_0 - 7\pi/4$ (solid line) with gains $\gamma = 1,\ h = 2,\ \beta = 2.91$.

The convergence to zero of α, θ, ϕ, u and c for the two paths reported in figure (5.5) is shown in figures (5.6) and 5.7). The developed control strategy can be adopted either for path tracking of a given 2D curve, or to navigate among via points or to design an autonomous navigation algorithm: a simple path tracking controller can be realized assuming that the target state space point $(0,0,0)$ moves along the desired curve. This approach has been analyzed by Aicardi et al.[2] for the unicycle model (equation (5.3)) with the control law given by equations (5.4) and (5.5) and can be extended to the kinematic model equation (5.7) controlled by equations (5.15) with minor changes. As far as autonomous navigation is concerned, the proposed control strategy is appealing being globally convergent and requiring only position and orientation errors that can be reasonably measured by standard on board vehicle sensors. Yet for a practical implementation on real systems two aspects of the proposed control law must be considered: the maximum vehicles curvature radius and actuator saturation. The curvature upper bound constraint can be managed assuming to approach the target form a sufficiently

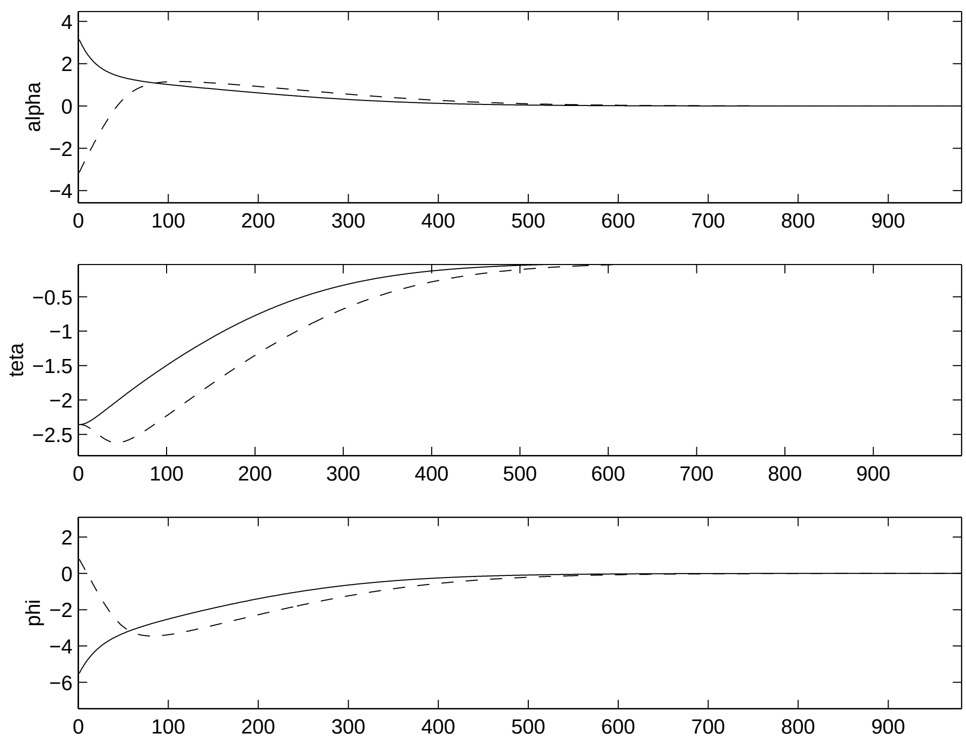

5.6.Convergence of α, θ, ϕ for the paths starting in (1,1) with initial orientation $\phi_0 = \pi/4$ (dashed lines) and $\phi_0 = -7\pi/4$ (solid lines).

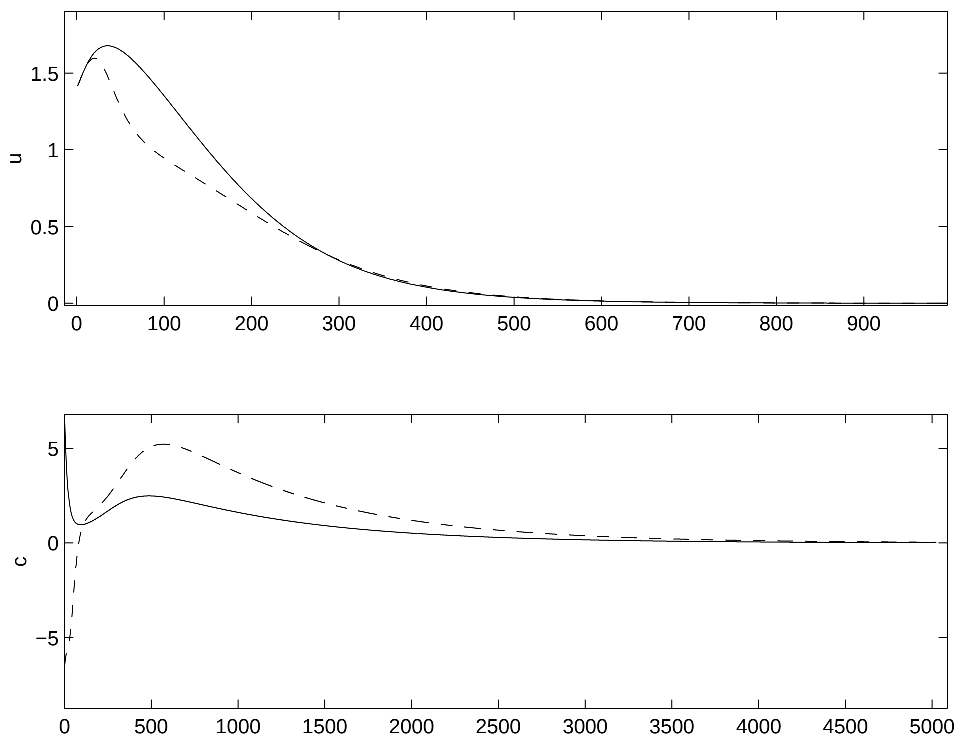

5.7.Convergence of c and u for the paths starting in $(1, 1)$ with initial orientations $\phi_0 = \pi/4$ (dashed lines) and $\phi_0 = -7\pi/4$ (solid lines). Notice the different time scales of the convergence of u and c.

distant point. As discussed above, if α converges to a region where $\sin\alpha \simeq \alpha$ being e greater then some limit $e^*(\alpha_0, \theta_0, \bar{c})$, then c will converge to zero without ever exceeding some prescribed upper bound $\bar{c}$. Actuator saturation must be considered with reference to the proportional control law $u = \gamma e$ equation (5.8). Notice that as long as γ is strictly positive, the value of γ does not affect the convergence properties of the state (as h and β do) but only the convergence rate, so one could argue that choosing γ sufficiently small can always avoid saturation problems. Indeed in some applications, as the path tracking problem where the moving target is always reasonably close, this is the most simple way of dealing with saturation, but in other circumstances, as autonomous navigation on long distances, it is not. The point is then to understand if and how actuator saturation due to $u = \gamma e$ affects the convergence of the state to the target $(0,0,0)$ and eventually design a different bounded control law for u. Actuator saturation occurring with a straight forward implementation of equations (5.15) can be modelled as:

$$u = \gamma e \; sat(\gamma e, \bar{u}) : \gamma > 0 \tag{5.19}$$

being sat a discontinuous function defined as

$$sat(x,y) = \begin{cases} 1 \; \forall \; |x| < y \\ \frac{y}{|x|} \; \forall \; |x| \geq y \end{cases} \quad \forall \; y > 0 \tag{5.20}$$

that models a *hard* saturation of u. With only marginal technical differences related to the discontinuity of $sat(\gamma e, \bar{u})$ for $\gamma e = \bar{u}$, the whole control law design procedure going form equation (5.9) to equation (5.15) can be replicated replacing $\gamma e \; sat(\gamma e, \bar{u})$ to γe: as a result equations (5.9), (5.11), (5.13) and (5.14) should be multiplied by $sat(\gamma e, \bar{u})$ and this will not affect either the global stability properties or the convergence analysis of $c \to 0$ developed for the unsaturated case as long as e is finite and $\bar{u} > 0$ (obvious). Indeed this is a satisfactory result as it suggest that a straight forward implementation of equations (5.15) will guarantee convergence even in presence of a *hard* saturation on u as the one modelled by equation (5.19). As an example the simulation shown in figure (5.5) relative to the starting configuration $(1, 1, -7\pi/4)$ with gains $\gamma = 1$, $h = 2$, $\beta = 2.91$ has been repeated with the same gains saturating the linear velocity u to 0.5, i.e. $\bar{u} = 0.5$ in equation (5.19). The resulting path and the values of α, θ, ϕ, u and c for the saturated and unsaturated cases are reported in figures (5.8) and (5.9). Another way of approaching the saturation problem is to choose a smooth and bounded control law for u compatible with the actuator dynamics. Perhaps the most simple choice is to compute u as:

$$u = \frac{\gamma e}{\dfrac{e}{a} + 1} \tag{5.21}$$

so that, as shown in figure (5.10), u is smooth (*soft* saturation), bounded by γa and linear in e when $e \ll a$. Replacing equation (5.21) in equation (5.9) and computing V

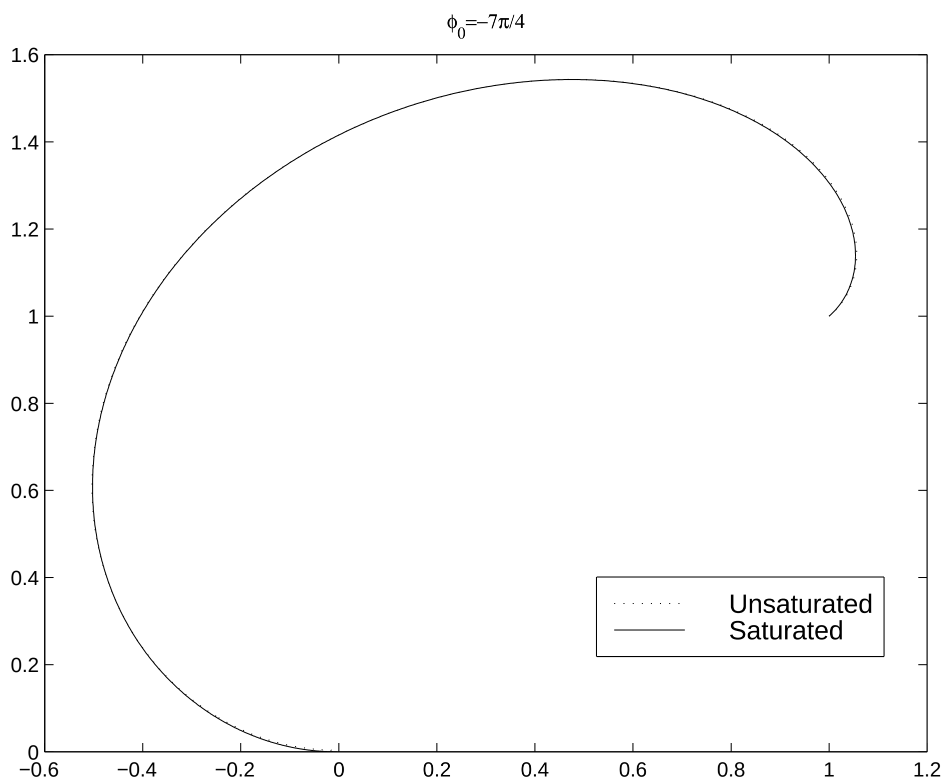

5.8.Paths with saturated (solid line) and unsaturated (dashed line) u. Refer to text for details.